Biomaterials 219 (2019) 119368

Contents lists available at ScienceDirect

Biomaterials

journal homepage: www.elsevier.com/locate/biomaterials

Size and temporal-dependent efficacy of oltipraz-loaded PLGA nanoparticles for treatment of acute kidney injury and fibrosis

Hang Yu[a,b,1], Tingsheng Lin[a,b,1], Wei Chen[a,b], Wenmin Cao[a,b], Chengwei Zhang[a,b], Tianwei Wang[a,b], Meng Ding[a,b], Sheng Zhao[c], Hui Wei[c,***], Hongqian Guo[a,b,**], Xiaozhi Zhao[a,b,*]

[a] Department of Urology, Nanjing Drum Tower Hospital, Medical School of Nanjing University Nanjing, Jiangsu, 210008, China
[b] Institute of Urology, Nanjing University, Nanjing, Jiangsu, 210008, China
[c] Department of Biomedical Engineering, College of Engineering and Applied Sciences, Nanjing National Laboratory of Microstructures, Jiangsu Key Laboratory of Artificial Functional Materials, Nanjing University, Nanjing, Jiangsu, 210093, China

ARTICLE INFO

Keywords:
Drug delivery
Nanomedicine
Acute renal injury
Renal fibrosis
Nanoparticles

ABSTRACT

Acute kidney injury (AKI) is associated with high mortality and morbidity with no effective treatment available at present, which greatly escalates the risk of chronic kidney disease. Nanotechnology-based drug delivery for targeting renal tubules offers a new strategy for AKI treatment but remains challenging due to the glomerular filtration barrier. To tackle this challenge, here we demonstrate that poly (lactic-co-glycolic acid) (PLGA) nanoparticles (NPs) of 100 nm diameter could selectively accumulate in mouse injury kidneys in correlation to the degree of kidney injury and administration time during the initial phase of renal ischemia-reperfusion injury. The NPs were located in renal tubular epithelial cells confirmed by immunofluorescence, which is critical for the progression of AKI. Taking advantage of the high accumulation and renal tubule targeting of the PLGA NPs in the ischemia-reperfusion (IR) kidney, we designed PLGA NPs loaded with Oltipraz (PLGA-Oltipraz NPs) to treat IR-induced AKI and renal fibrosis. *In vitro* results showed that compared to free Oltipraz, PLGA-Oltipraz NPs displayed a higher antioxidation effect with improved cell viability, lower contents of malondialdehyde, and higher activity of superoxide dismutase. The therapeutic efficacy of PLGA-Oltipraz NPs was further investigated *in vivo*. Mice with AKI treated with PLGA-Oltipraz NPs exhibited significantly reduced tubular necrosis, less collagen deposition, and better renal function at the initial phase as well as improved renal fibrosis at the recovery phase. This study establishes a promising approach for AKI and fibrosis treatment with PLGA-Oltipraz NPs. It also reveals the importance of size-selective NPs and drug administration time window to nanotherpeutics.

1. Introduction

Acute kidney injury (AKI) is a common and serious clinical disorder with high morbidity and mortality [1–3]. It occurs in 3.2%–9.6% of hospitalized patients and is responsible for about 2 million deaths per year worldwide with increasing incidence [4]. AKI causes microcirculatory disturbances, excessive production of reactive oxygen species and inflammatory factors, which give rise to the renal tubular injury [5,6]. This further stimulates the activation of interstitial fibroblasts, triggers extracellular matrix deposition in the interstitium, results in renal fibrosis, and eventually leads to chronic kidney disease (CKD) [7,8]. AKI, while has attracted much attention from nephrologists, still lacks specific and effective clinical treatments [9].

The development of nanotechnology sheds light on AKI treatment [10,11]. The nanoparticles (NPs)-based delivery system contributes to the pharmacokinetics and bio-distribution of drugs and facilitates targeted drug delivery to specific organs [12–15]. However, the use of the NPs-based system to deliver drugs to renal tubules is challenged by the glomerular filtration barrier (GFB) [16,17]. Under the physiological condition, water and small solutes (such as urea and glucose) in plasma

* Corresponding author. Department of Urology, Nanjing Drum Tower Hospital, Medical School of Nanjing University, Institute of Urology, Nanjing University, Nanjing, Jiangsu, 210008, China.
** Corresponding author. Department of Urology, Nanjing Drum Tower Hospital, Medical School of Nanjing University, Institute of Urology, Nanjing University, Nanjing, Jiangsu, 210008, China.
*** Corresponding author. Department of Biomedical Engineering, College of Engineering and Applied Sciences, Nanjing National Laboratory of Microstructures, Jiangsu Key Laboratory of Artificial Functional Materials, Nanjing University, Nanjing, Jiangsu, 210093, China.
E-mail addresses: zhaoxz@nju.edu.cn (X. Zhao), dr.ghq@nju.edu.cn (H. Guo), weihui@nju.edu.cn (H. Wei).
[1] These authors contributed equally to this work.

https://doi.org/10.1016/j.biomaterials.2019.119368
Received 15 January 2019; Received in revised form 8 July 2019; Accepted 14 July 2019
Available online 16 July 2019

are able to cross the GFB into the urine, while high-molecular-weight plasma components are retained in the blood [18]. Only a few nanomaterials were reported to target renal tubules. For instance, carbon nanotubes with a diameter of 5 nm were used for targeted drug delivery to renal tubules in a cisplatin-induced AKI model [19]. The carbon nanotubes loaded with Trp53 siRNA and Mep1b siRNA could effectively alleviate kidney damage and renal tubular inflammation. Catechol-derived chitosan NPs with a diameter of 40 nm could target renal tubules and interstitium, reducing the occurrence of renal fibrosis in the unilateral ureteral occlusion model [20]. Shaped DNA origami nanostructures had superiority of accumulation in mice kidneys. Besides, rectangular DNA origami nanostructures possessed renal-protective properties in AKI mouse model [21]. Nevertheless, these materials are still far away from clinical application. More effective nanomaterials for targeting renal tubules are required.

Renal ischemia-reperfusion injury (RIRI) is one of the most frequent causes of AKI [22]. Previous reports showed that the structure and permeability of GFB were significantly changed in the RIRI animal model at the initial phase, which may allow for NPs to pass through [23–25]. Therefore, we reasoned that it would be possible to design NPs with a specific size to cross the impaired GFB, which would in turn enable the targeted drug delivery to renal tubules. In the present study, taking poly (lactic-co-glycolic acid) (PLGA) as the model, we found that PLGA NPs of 100 nm could accumulate in the ischemia-reperfusion (IR) kidney and target renal tubular epithelial cells at a specific administration time. The NPs accumulation was closely related to the degree of kidney injury and administration time of NPs. To further validate our hypothesis, we loaded Oltipraz, a drug for AKI and renal fibrosis treatment, into PLGA NPs of 100 nm to prepare the PLGA-Oltipraz NPs, which were intravenously delivered to the IR-induced AKI-to-CKD mouse model [26–28]. We found that the PLGA-Oltipraz NPs could specifically target the IR kidney at the initial phase and continuously release Oltipraz for effective treatment of AKI and renal fibrosis (Scheme 1).

2. Materials and methods

2.1. Fabrication of PLGA NPs

The PLGA NPs of about 100 nm in diameter were prepared as follows [29,30]. 5 mg PLGA (Poly(D,L-lactide-co-glycolide) (lactide:glycolide 50:50, ester terminated, molecular weight is 38,000–54,000, Sigma-Aldrich, St. Louis, MO, USA) was dissolved in acetonitrile (2 mL). DiR (Thermo Fisher Scientific, MA, USA), a cytomembrane dye, was then added to PLGA acetonitrile solution. Lecithin (soybean, refined, molecular weight: ~330 D) and DSPE-PEG (1,2-distearoyl-snglycero-3-phosphoethanolamine-N-carboxy(polyethylene glycol) 2000) were purchased from Sigma-Aldrich (St. Louis, MO, USA). Lecithin (1.5 mg) and DSPE-PEG (5 mg) were dissolved in 20 mL of distilled water. Then the PLGA and DiR mixed acetonitrile solution was slowly added dropwise to the rapidly stirred lecithin and DSPE-PEG solution. To evaporate the acetonitrile, we further stirred the obtained solution overnight at room temperature. Then the obtained NPs suspension was ultrafiltered by using a Millipore Amicon centrifuge tube (molecular weight ~100 kD) and washed twice to completely remove the organic solvent. The obtained NPs solution was resuspended in PBS with a PLGA concentration of 5 mg/mL, then the PLGA NPs dispersion was stored at 4 °C.

In order to prepare PLGA NPs with the size about 200 nm, 10 mg PLGA was dissolved in 1 mL acetonitrile solution. Lecithin (1 mg) and DSPE-PEG (2 mg) were dissolved in 20 mL of distilled water. Remaining steps were the same as for 100 nm PLGA NPs.

In order to prepare PLGA NPs with the size about 300 nm, 20 mg PLGA was dissolved in 1 mL acetonitrile solution. Lecithin (0.5 mg) and DSPE-PEG (1 mg) were dissolved in 10 mL of distilled water. Remaining steps were the same as 100 nm PLGA NPs.

2.2. Preparation of PLGA-Oltipraz NPs

PLGA-Oltipraz NPs of 100 nm in diameter were prepared as follows. PLGA (5 mg) was dissolved in acetonitrile (2 mL). Oltipraz (25 μg, Selleck, Shanghai), a Nrf2 activator was added to 2 mL of PLGA acetonitrile solution and thoroughly mixed at room temperature. DSPE-PEG (5 mg) and Lecithin (1.5 mg) were dissolved in 20 mL of distilled water. Then the PLGA and Oltipraz acetonitrile solution was slowly added dropwise to the rapidly stirred lecithin and DSPE-PEG solution, and then stirred overnight at room temperature. The prepared nano-suspension was ultrafiltered, centrifuged by using a Millipore Amicon centrifuge tube (molecular weight 100 kD) and washed twice to completely remove the organic solvent. The obtained NPs solution was resuspended in 1 mL PBS to produce PLGA-Oltipraz NPs solution.

2.3. Characterization of PLGA and PLGA-Oltipraz NPs

The morphology and particle size of NPs were evaluated by transmission electron microscopy (TEM; Hitachi H-7650). Dynamic light scattering (DLS; Brookhaven Instruments Corp., USA) was employed to measure the hydrodynamic size and zeta potential of NPs. Oltipraz concentration and loading capacity of NPs were determined by UV–visible spectra with a UV–visible spectrophotometer (UV2450,

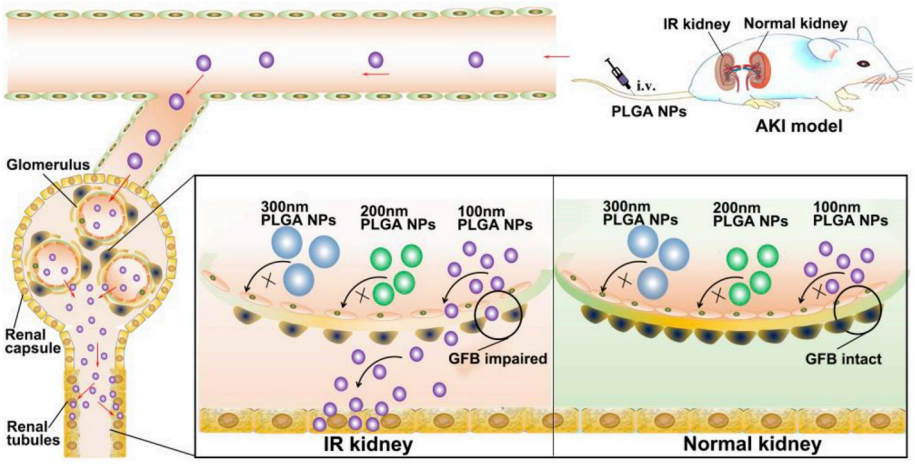

Scheme 1. Application of PLGA-Oltipraz nanoparticles (NPs) with particle size of 100 nm in ischemia-reperfusion (IR) induced acute kidney injury (AKI). GFB, glomerular filtration barrier; i.v., intravenous injection.

Shimadzu Corp.).

2.4. In vitro cellular uptake behavior of PLGA NPs

Human renal tubular epithelial cell line (HK2) was purchased from Cell Bank of Shanghai Institutes for Biological Sciences. HK2 cells were cultured in DEME medium containing 10% fetal bovine serum (Wisent, Nanjing, China), 1% penicillin-streptomycin (Gibco, MA, USA) and incubated in 5% CO_2 at 37 °C in a water-saturated atmosphere. Cells were seeded in 6-well plates with a density of 5×10^5 cells/well, and cultured for 24 h. To evaluate the cellular uptake of PLGA NPs by flow cytometry, fresh medium containing 1 mg PLGA NPs (labeled with DiR, 2.5 μg/mL) with different sizes were added. After 6 h co-incubation, cells were washed with phosphate buffered saline (PBS) three times and centrifuged, re-suspended in 500 μL of PBS, and analyzed by flow cytometry. The fluorescence of DiR was collected on the APC-Cy7-H channel.

2.5. In vitro anti-oxidative stress effect of PLGA-Oltipraz NPs

HK2 cells were seeded in two cell culture plates and cultured with DMEM containing 10% (v/v) FBS, pH 7.2, at 37 °C with 5% CO_2. Cells were pre-treated separately with DMSO, PLGA NPs, PLGA-Oltipraz NPs, and free-Oltipraz, then cultured for 24 h. The concentration of Oltipraz in groups with free Oltipraz, and PLGA-Oltipraz NPs was 20 μM. Cells in one plate were cultured in serum-starved medium and exposed to hypoxia for 1 h, then cultures were replaced with standard medium and allowed to recover in room air with 5% CO_2 for 1 h. Cells in another plate were cultured under normal conditions for 2 h. Cell lysates were prepared for subsequent experiments. Western blot analysis of the protein levels of Nrf2 (#12721, 1:1000, Cell Signaling Technology, Danvers, MA, USA), NQO1 (ab80588, 1:2000, Abcam, Cambridge, UK) and α-Tubulin (sc-73242, 1:5000, Santa Cruz). To examine malondialdehyde (MDA) and superoxide dismutase (SOD) generated by hypoxia condition, thiobarbituric acid was used to measure MDA, WST-8 assay kit (Beyotime Biotech, Shanghai, China) was used to examine SOD generation. And CCK-8 assay kit (Vazyme biotech, Nanjing, China) was used to assess cell viability. Briefly, cell lysis samples were first incubated with a working solution for an indicated time, followed by detection in a spectrophotometer system (TECAN). The total protein concentration of each sample was determined by the BCA Protein Assay Kit (Vazyme biotech, Nanjing, China), and was used to normalize the measured MDA and SOD results.

2.6. AKI-to-CKD mice model

All animal experimental protocols were approved by the Institutional Animal Care and Use Committee, Drum Tower Hospital, Medical School of Nanjing University. ICR Mice (6–8 weeks) were anesthetized with isoflurane inhalation, and injected buprenorphine subcutaneously for analgesia. AKI-to-CKD mice model was established by unilateral renal pedicle clamping for 45 min followed by reperfusion as described previously [31]. In brief, we firstly removed the left renal hilus fat and isolated the renal vessels completely, then placed the mice on a 38 °C heating plate and clamped renal pedicle with vascular bulldog clamps for 45 min. Whereafter, we released the bulldog clamp slowly, and observed that the color of the left kidney changed from purple-black to red, indicating successful reperfusion. In the sham group, we isolate the left renal pedicle without clamping it.

2.7. In vivo bio-distribution of PLGA NPs

A PerkinElmer IVIS Spectrum small-animal *in vivo* imaging system was used to measure the fluorescence intensity of NPs. The near-infrared (NIR) fluorescent image parameters were preset by using DiR dye, with excitation wavelength at 745 nm and emission wavelength at 800 nm. The fluorescence intensity of the images was normalized.

To study the relation between NPs size and their bio-distribution, DiR labeled PLGA NPs (200 μL, 5 mg/mL PLGA) of the three different particle sizes was intravenously injected in the RIRI mouse model immediately after RIRI. Three mice from each group were sacrificed by CO_2 asphyxiation at 3, 6, 12, 24, and 48 h after injection. Hearts, livers, spleens, lungs, and kidney tissues were removed and the surface of the organs was floated/cleaned with physiological saline, then blotted dry. The organs were photographed and the NIR fluorescent signals were measured.

To investigate the effect of NPs administration timing on NPs bio-distribution, RIRI mice were divided into six groups with different timing of NPs administration. DiR labeled NPs (200 μL, 5 mg/mL PLGA) was administered at 0 h, 12 h, 24 h, 48 h, and 72 h and 7 d after RIRI. Three mice from each group were sacrificed at 3, 6, 12, 24, and 48 h after injection, and then the major organs were removed to perform NIR imaging.

To explore the relationship between the degree of injury in the RIRI kidney and the accumulation of NPs, mice were divided into four groups by the blocking time of the left kidney vessels: 15, 30, 45, and 60 min. DiR labeled NPs (200 μL, 5 mg/mL PLGA) was intravenously injected immediately after RIRI. Three mice from each group were sacrificed at 3, 6, 12, 24 and 48 h after injection. The major organs were then harvested for NIR imaging.

2.8. Location of the accumulated PLGA NPs in injured kidney

To revalidate that the PLGA NPs can target the IR kidney, IR kidneys with NPs accumulation illustrated by the *in vivo* imaging system were fixed in OCT gel and frozen at − 20 °C, and frozen sections of 5-μm thick were prepared. Then, tissue sections were incubated with 3% bovine serum albumin (BSA)/0.3% Triton X-100 for 15 min at room temperature. After removing the solution, sections were incubated at room temperature with fluorescein-labeled *Phaseolus vulgaris* erythroagglutinin (PHA-E (1:200), FL-1121, Vector Laboratories, Peterborough, UK) or *Arachis hypogaea* lectin (PNA (1:100), L7381, Sigma-Aldrich, St. Louis, MO, USA) for 1 h. After rinsing with PBS three times, the core was incubated with 4′, 6-dia- midino-2-phenylindole (DAPI, Beyotime Biotechnology, Shanghai), and fluorescence was observed by fluorescence microscope.

2.9. Therapeutic efficacy of PLGA-Oltipraz NPs in the AKI-to-CKD mice model

In the established ischemia reperfusion induced AKI model, the mice were divided into eight groups (9 mice/group) for treatment: Sham, Sham + PLGA NPs, Sham + Oltipraz, Sham + PLGA-Oltipraz NPs, IR, IR + PLGA NPs, IR + Oltipraz, and IR + PLGA-Oltipraz NPs. PBS, PLGA NPs, Oltipraz, and PLGA-Oltipraz NPs were intravenously injected in the Sham and IR groups immediately. The dose of Oltipraz in groups with free Oltipraz, and PLGA-Oltipraz NPs was 5 μg. The day of administration was set as 12 h. Three mice in each group were executed on day 3, 7, and 42 (6 weeks). Kidneys and other primary organs were harvested for hematoxylin and eosin (H&E) staining. Tissue sections (5 μm) were stained with H&E and Masson trichrome (Solarbio Life Sciences, Beijing). The staining results were measured and scored to assess the degree of injury. The final score reflected the degree of cast formation, tubular necrosis, loss of brush border, and tubular dilation in 10 randomly selected, non-overlapping fields (200 ×) as follows: 0, none; 1, ≤10%; 2, 11–25%; 3, 26–45%; 4, 46–75%; and 5, ≥76%.

Kidney sections were also used for IHC staining to detect the expression of extracellular matrix proteins. IHC was performed using paraffin-embedded sections according to standard protocols of Cell Signaling Technology. The antibodies used for IHC were as follows: α-smooth muscle actin (α-SMA; Abcam, Cambridge, UK, ab5694, 1:3000), collagen I (Abcam, ab34710, 1:400), and fibronectin (Abcam, ab2413,

1:400) DAB (ZSGB-BIO, Beijing) was used as an HRP-specific substrate. Photographs of representative fields were captured under high-power magnification (× 200) by using Leica LAS v4.12 software. The positive areas in each image were counted and analyzed with Image-Pro Plus v6.0.

2.10. Western blot analysis

To examine the expression of Nrf2 signaling pathway-associated proteins, protein was extracted from tissues and cells and underwent Western blot analysis as previously described [32]. The antibodies used were as follows: Anti-Nrf2 antibody (Cell Signaling Technology, Danvers, MA, USA, #12721, 1:1000), anti-NQO1 antibody (Abcam, ab80588, 1:2000), anti-Gpx2 antibody (Abcam, ab137431, 1:1000), anti-GCLC antibody (Proteintech, Rosemont, IL, USA, 12601-1-AP, 1:2000), and anti-α-Tubulin antibody (Santa Cruz, sc-73242, 1:5000).

2.11. Measurement of renal function

To investigate the renal function protection effect of PLGA-Oltipraz NPs, the AKI mouse model was established by blocking the left kidney blood vessel for 45 min and resecting the right kidney after the release of the left blood vessel clamp, while the sham group underwent the right kidney resecting without the left pedicle clamping. Then, the AKI mouse model and sham operation mice were divided into eight groups (5 mice/group) for treatment: Sham + PBS, Sham + PLGA NPs, Sham + Oltipraz, Sham + PLGA-Oltipraz NPs, IR + PBS, IR + PLGA NPs, IR + Oltipraz, and IR + PLGA-Oltipraz NPs. PBS, PLGA NPs, Oltipraz, and PLGA-Oltipraz NPs were intravenously injected in the Sham and AKI groups immediately. The dose of Oltipraz in groups with free Oltipraz, and PLGA-Oltipraz NPs was 5 μg. After 24 h, mice were sacrificed and blood samples were harvested. The serum was separated by centrifuging blood samples and stored at −80 °C until analysis of BUN and serum creatinine. BUN and creatinine assay kits were purchased from BioAssay System (Hayward, USA).

2.12. Statistical analysis

Statistical analysis involved two-sided Student's *t*-test for two groups and one-way ANOVA for multiple groups. $P < 0.05$ was considered statistically significant.

3. Results and discussion

3.1. Characterization of PLGA NPs

PLGA NPs with different particle size labeled with DiR were prepared. Fig. 1a-c exhibits the particle size distribution, transmission electron microscope (TEM) images of different NPs, and the flow cytometry results of the obtained PLGA NPs in human renal tubular epithelial cells (HK2 cells). Dynamic light scattering (DLS) showed that the mean size of the PLGA NPs fabricated at 100, 200, and 300 nm was 100 ± 14.1, 200 ± 19.5 and 300 ± 20.8 nm, respectively (Fig. 1a), and the PDI was 0.098 ± 0.009, 0.112 ± 0.015, and 0.156 ± 0.027, respectively. TEM revealed that all the three NPs formed by self-assembly were generally spherical in shape and showed good mono-dispersity (Fig. 1b). Next, we investigated the cellular uptake efficiency of PLGA NPs by incubating HK2 cells with the three sizes of NPs for 4 h. The three PLGA-DiR NPs had similar cellular uptake behaviors observed from flow cytometry (Fig. 1c).

3.2. Bio-distribution of PLGA NPs

We investigated the relationship between the particle size and their accumulation in the IR kidney after administration of PLGA-DiR NPs with three particle sizes. IR-induced AKI-to-CKD mouse model was established by unilateral renal pedicle clamping for 45 min followed by reperfusion as described previously [31]. PLGA-DiR NPs with the three different particle sizes (100 nm, 200 nm and 300 nm) and free DiR were intravenously injected immediately after the model was established, respectively. The near-infrared (NIR) fluorescence of the mouse IR kidney and contralateral kidney was observed at 3, 6, 12, 24, and 48 h post-injection. The semiquantitative analysis of NIR fluorescence in IR kidneys at 48 h post-injection showed that the relative fluorescence intensity of 100 nm PLGA NPs, 200 nm PLGA NPs, 300 nm PLGA NPs and free DiR was 39%, 7%, 4% and 2%, respectively. PLGA NPs of 100 nm significantly accumulated in IR kidneys, whereas NPs of 200 and 300 nm were barely accumulated (Fig. 1d and e). Thus, the kidney-targeting property of PLGA NPs was closely related to particle size. On the other hand, all contralateral kidneys showed negligible DiR fluorescence. This was probably due to the impaired GFB after the RIRI, which enabled large molecules to pass through [33,34]. Meanwhile, the permeability of GFB at the contralateral kidney was not changed by RIRI. Therefore, PLGA NPs with different particle size could not accumulate in the contralateral kidneys. We also noted that no NIR fluorescence was detected in IR kidneys or contralateral kidneys after free DiR injection (Fig. 1d). The possible reason is still under investigation and will be reported in due course.

To evaluate the bio-distribution of PLGA NPs *in vivo*, we intravenously injected 200 μL of 100 nm PLGA NPs (0.05 mg/mL) in RIRI mice, and then imaged them by a NIR imaging system. Among major organs excised at different timepoints post-injection, strong DiR fluorescence intensity appeared in the IR kidney, whereas the contralateral kidney showed negligible DiR fluorescence (Fig. 1f). The relative fluorescence intensity in IR kidneys at 3 h, 12 h, 24 h, 48 h, 72 h, 7 days and 10 days post-injection was 45%, 31%, 32%, 32%, 41%, 52% and 70%, respectively (Fig. 1g). The results revealed that PLGA NPs could specifically target the IR kidney. At day 10 after injection, the fluorescence from PLGA NPs was still evident in IR kidney, indicating PLGA NPs could stay in the IR kidney for at least 10 days, thus enabling the continuous release of the encapsulated drugs.

Next, we investigated the effect of administration timing on the accumulation of NPs in the IR kidney. The PLGA-DiR NPs of 100 nm were administered at 0 h, 12 h, 24 h, 48 h, 72 h, and 7 days after the establishment of the RIRI model. At 3, 6, 12, 24, and 48 h after administration, the major organs of mice were excised for NIR imaging. Fig. 2a exhibits the NIR fluorescence images of kidneys. At 48 h NIR imaging, the relative fluorescence intensity of IR kidney at 0, 12, 24, 48 and 72 h NPs administration was 18, 17.5, 7, 5.5, and 4 times higher than that at 7 days NPs administration, respectively (Fig. 2a and b). The relative fluorescence intensity of IR kidney was significantly higher at 0 h and 12 h administration while gradually decreased with the delayed administration. Therefore, the accumulation of PLGA NPs in the IR kidney is reversely correlated with increased administration timing. Overall, substantial accumulation of NPs occured even when the administration was given within 72 h after RIRI.

We further explored the effect of the degree of injury of the IR kidney on the accumulation of NPs. The RIRI mice were divided into five groups by ischemic time of left kidneys: 0 (sham-operated group), 15, 30, 45 and 60 min, respectively. The PLGA-DiR NPs of 100 nm were administered immediately after surgery, at 3, 6, 12, 24 and 48 h, the major organs of mice were excised for NIR imaging. The relative fluorescence intensity at 48 h in IR kidneys of 0, 15, 30, 45 and 60 min ischemic time was 2%, 2%, 5%, 39%, and 37%, respectively. PLGA NPs accumulation was barely observed in groups with an ischemic time of 15 and 30 min, indicated by very low fluorescence intensity. However, with the ischemic time of 45 and 60 min, the accumulation of PLGA NPs in IR kidneys was significantly increased, reflected by the relatively high fluorescence intensity (Fig. 2c and d). We reason that the degree of injury is an important factor affecting the accumulation of NPs in IR kidneys. These results suggest that mild renal injury may not significantly change the structure and permeability of GFB and prevent the

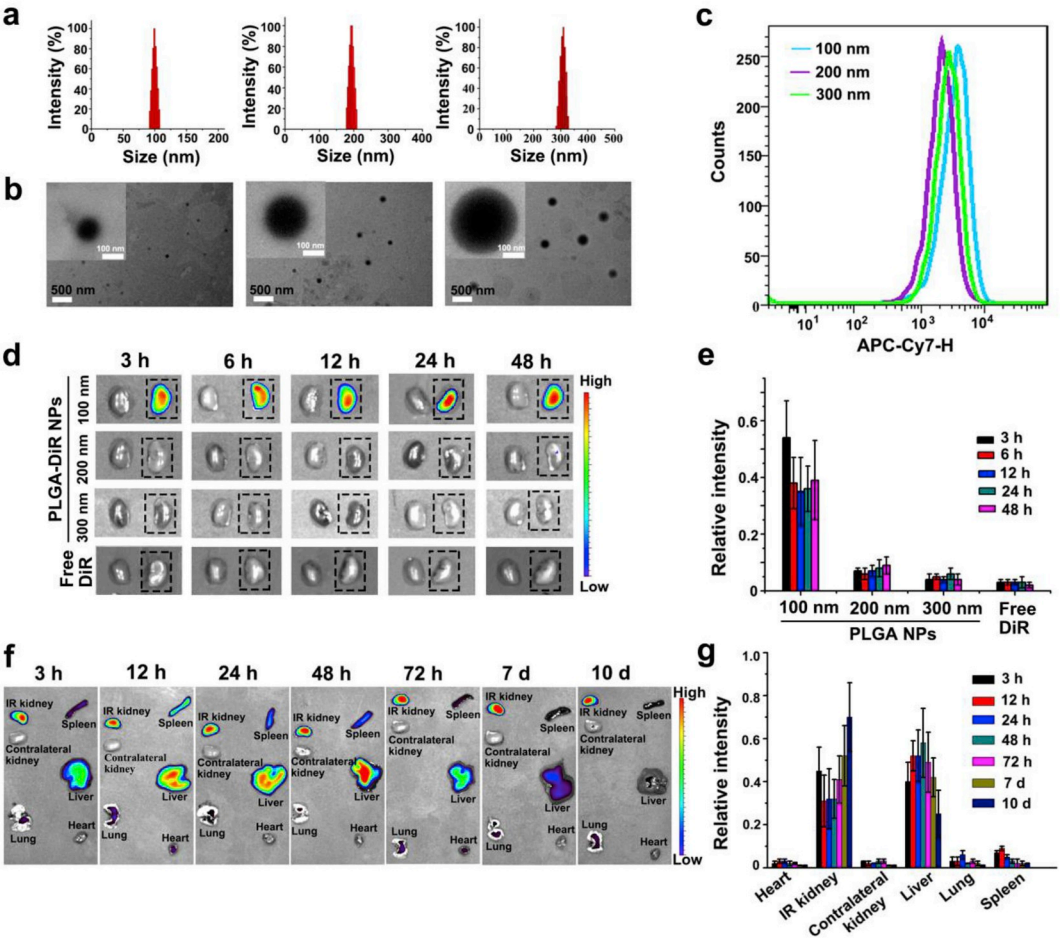

Fig. 1. The characterization and *in vivo* bio-distribution of PLGA NPs. (a) Size distribution of PLGA NPs by dynamic light scattering. (b) Transmission electron microscopy (TEM) images of PLGA NPs. Scale bar, 500 nm. (c) Flow cytometry of HK2 cells incubated with PLGA NPs of different sizes. (d) PLGA NPs with different particle sizes and free DiR were intravenously injected in renal ischemia-reperfusion injury (RIRI) model of mice immediately after surgery. NIR fluorescence images of ischemia-reperfusion (IR) kidneys (dotted box) and contralateral kidneys of RIRI mouse at the indicated time after injection. (e) Semi-quantitative bio-distribution of PLGA NPs in IR kidneys from (d). (f) NIR fluorescence images of major organs after injection of PLGA NPs with particle size of 100 nm. (g) Semi-quantitative bio-distribution of PLGA NPs in RIRI mouse model by mean PLGA NPs fluorescence intensity in organs from (f). The data are shown as mean ± SD (n = 3).

NPs from passing through. However, the kidney will get fully recovery from mild ischemia-reperfusion injury and will not progress to renal fibrosis.

3.3. Localization of PLGA NPs

We observed the accumulation of 100 nm PLGA NPs in the IR kidney. To further identify the exact location of PLGA NPs in the IR kidney, we applied immunofluorescence analysis to kidney frozen sections. IR kidney sections were stained with phytohemagglutinin-E (PHA-E) to label proximal convoluted tubules while phytoagglutin (PNA) was used to label distal convoluted tubules, respectively [35]. DiR fluorescence was mainly observed in proximal and distal convoluted tubule cells in the IR kidney, while DiR fluorescence was negligible in the contralateral kidney or sham control kidney (Fig. 3a and b). It has been reported that renal tubular epithelial cells play important roles in the progression and recovery of AKI [7]. Tubular epithelial cells were observed to arrest at G2/M and adopt a profibrotic phenotype after AKI, leading to the progression of interstitial inflammation and fibrosis. Thus, repairing injured tubules to restore regular tubular function is of great significance in the treatment of AKI. In the present study, we demonstrated that PLGA-DiR NPs might directly target the proximal and distal convoluted tubules, which could contribute to drug delivery targeting the injured renal tubular epithelial cells.

3.4. Fabrication and characteristics of PLGA-Oltipraz NPs

We then constructed PLGA NPs encapsulating Oltipraz by using the method for 100 nm PLGA NPs. Oltipraz, a small molecule Nrf2 (nuclear factor erythroid 1-related factor 2) agonist, was chosen as the model drug because it regulates cell oxidative stress damage and has huge potential in the treatment of AKI and renal fibrosis [26–28]. Nrf2 is a nuclear transcription factor which binds to antioxidant response element and participates in modulating transcription and expression of antioxidant enzymes [36–38]. Though Oltipraz can easily pass through the GFB, maintaining an effective concentration in the renal tubules and interstitium is difficult [39,40]. Herein we constructed Oltipraz-loaded PLGA NPs to address this challenge. DLS confirmed the mean size of the PLGA-Oltipraz NPs as 100 ± 15.8 nm (Fig. 4a) with a PDI of 0.109 ± 0.012. TEM images showed that the self-assembled PLGA-Oltipraz NPs were generally spherical in shape. The UV–visible absorption spectrum of PLGA-Oltipraz NPs showed a characteristic absorption peak of Oltipraz at about 444 nm, indicating the successful encapsulation of Oltipraz (Fig. 4b). The loading capacity of Oltipraz was 1.1%. The zeta potential was −20 ± 6.7 mV (Fig. 4c). The release profile of Oltipraz from PLGA-Oltipraz NPs was evaluated. The cumulative release of Oltipraz reached 50% and 75% after 12 h and 4 days respectively, which indicated that drug release from PLGA NPs was a controlled-release process (Fig. 4d).

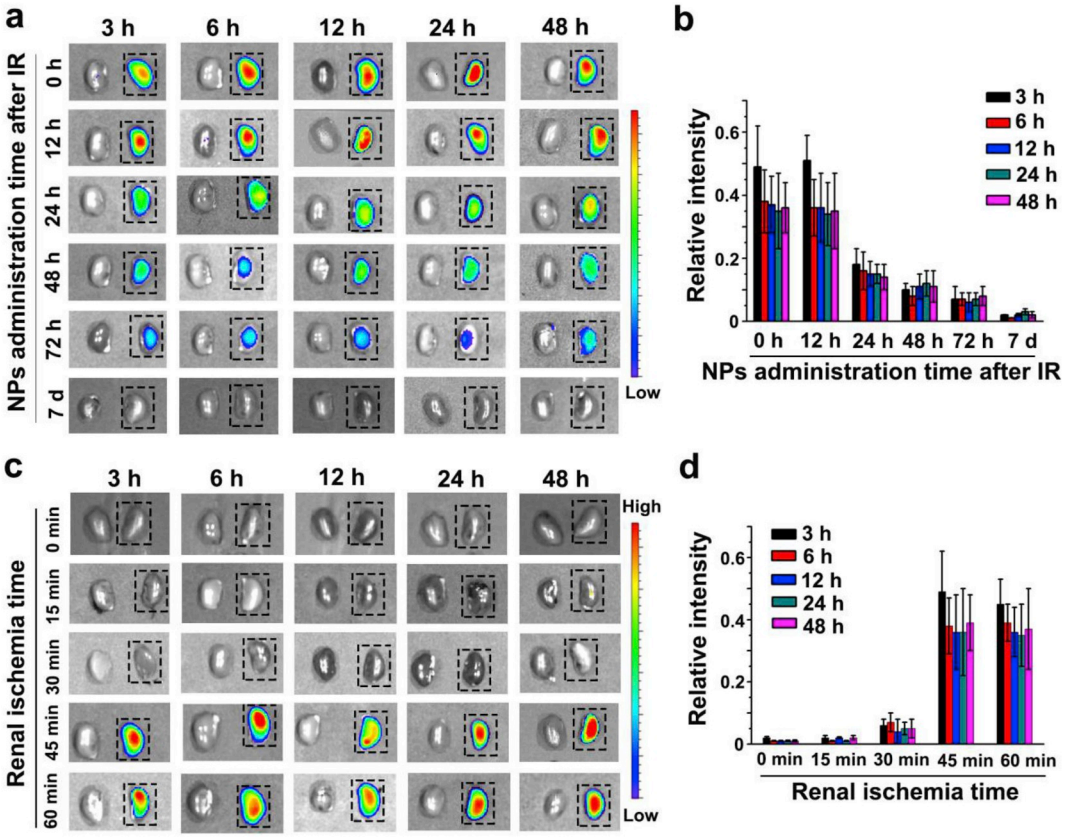

Fig. 2. PLGA NPs bio-distribution by NIR imaging. (a) The renal ischemia-reperfusion injury (RIRI) mice were intravenously injected with 100 nm PLGA NPs at the indicated time (0, 12, 24, 48, 72 h and 7 d) after surgery. NIR fluorescence images of ischemia-reperfusion (IR) kidneys (dotted box) and contralateral kidneys of RIRI mice at different times (3, 6, 12, 24, 48 h) after injection. (b) Semi-quantitative bio-distribution of PLGA NPs in IR kidneys from (a). (c) PLGA NPs with 100 nm particle sizes were intravenously injected in RIRI mice with different renal ischemia time (0, 15, 30, 45, 60 min) immediately after surgery. NIR fluorescence images of IR kidneys (dotted box) and contralateral normal kidneys at different times (3, 6, 12, 24, 48 h) after injection. (d) Semi-quantitative bio-distribution of PLGA NPs in IR kidneys from (c). The data are shown as mean ± SD (n = 3).

3.5. Antioxidant efficacy of PLGA-Oltipraz NPs in vitro

Next, we inspected the antioxidation effect of PLGA-Oltipraz NPs *in vitro*. Western blot assay was performed to analyze the expression levels of Nrf2 and NQO1. Under normal culture conditions, compared with PLGA and the DMSO control, both the PLGA-Oltipraz NPs and Oltipraz could activate Nrf2 and NQO1 expression, with PLGA-Oltipraz NPs exhibiting higher activation efficiency than Oltipraz alone (Fig. 4e). Under hypoxia and serum-free culture conditions, the expression of Nrf2 and NQO1 was inhibited. However, PLGA-Oltipraz and Oltipraz NPs conferred relatively higher expression of Nrf2 and NQO1 protein than the PLGA and DMSO control. The activation efficiency of the PLGA-Oltipraz NPs was better than Oltipraz alone in hypoxia and serum-free conditions. The malondialdehyde (MDA) content was 1.29 μmol/mg protein in PLGA-Oltipraz treated cells, while 1.62 μmol/mg protein in PLGA treated control cells ($p < 0.05$) during hypoxia (Fig. 4f). The superoxide dismutase (SOD) activity showed 1.02 U/mg protein in PLGA-Oltipraz treated cells, while 0.76 U/mg protein in PLGA treated cells ($p < 0.05$) in hypoxia (Fig. 4g). Moreover, the cell viability rate was 44.36% and 55.81% in PLGA and PLGA-Oltipraz treated cells in hypoxia condition ($p < 0.05$), respectively (Fig. 4h). PLGA-Oltipraz treatment conferred protection against hypoxia condition, as evidenced by lower contents of MDA, higher activity of SOD, and increased cellular activity when compared with PLGA and DMSO control cells (Fig. 4f, g, h).

3.6. Therapeutic efficacy of PLGA-Oltipraz NPs in vivo

Having achieved substantially high accumulation of PLGA NPs of 100 nm in the IR kidney, we next investigated the therapeutic efficacy of PLGA-Oltipraz NPs *in vivo*. RIRI mice were divided into eight groups for treatment: IR, IR + PLGA NPs, IR + Oltipraz, IR + PLGA-Oltipraz NPs, sham, sham + PLGA NPs, sham + Oltipraz and sham + PLGA-Oltipraz NPs. Mice in sham group underwent renal pedicle isolation without clamping. On day 3 after IR injury, IR, IR + PLGA NPs, and IR + Oltipraz kidneys showed a significantly higher degree of tubular damage on H&E staining, including cast formation, tubular necrosis, loss of brush border, and dilatation of tubules. However, mice treated with PLGA-Oltipraz NPs showed less tubular damage and the score of renal lesions was significantly reduced (Fig. 5a), which suggests the protective effect of PLGA-Oltipraz NPs on IR-induced renal injury. We then assessed renal fibrotic lesion area by Masson staining. PLGA-Oltipraz NPs administration markedly reduced collagen accumulation and deposition in the renal tubular interstitium; the fibrotic area was significantly lower than that with other treatments (Fig. 5a). To further determine the fibrotic lesions *in vivo*, we examined the expression of α-SMA, a marker of fibroblasts, collagen I, and fibronectin, representing extracellular matrix proteins, in renal tissues by IHC staining (Fig. 6a). In the IR + PLGA-Oltipraz NPs group, the expression of α-SMA, collagen I and fibronectin was significantly reduced (Fig. 6a). These results suggest a significant protective effect of PLGA-Oltipraz NPs on the IR kidney at the initial phase. Next, we further performed histological analysis of the IR kidneys at 6 weeks after RIRI and treatment. The score of renal fibrosis and fibrotic area (Fig. 5b), as well as α-SMA, collagen I,

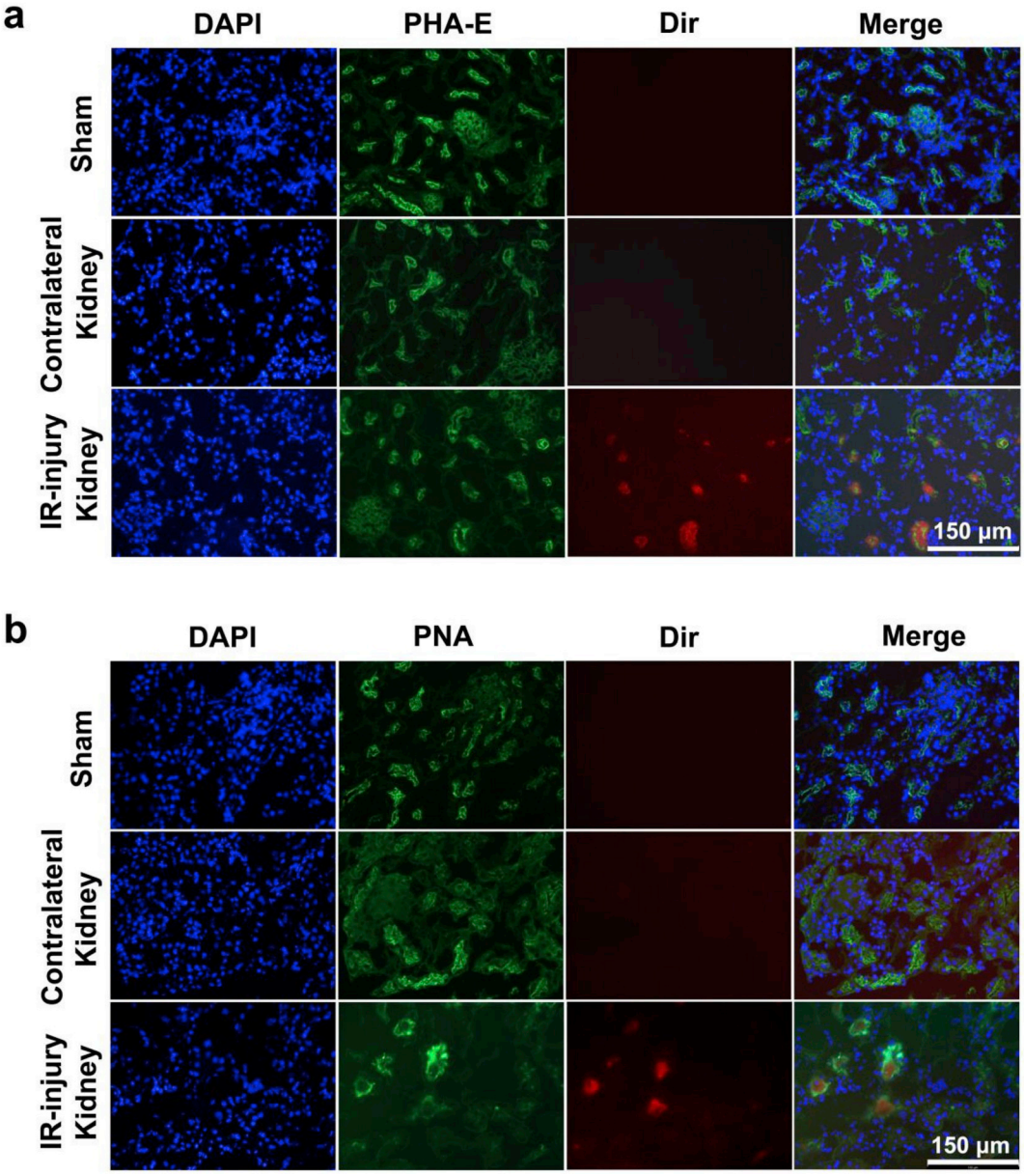

Fig. 3. Immunofluorescence analysis of PLGA-DiR NPs in IR-injured and contralateral kidneys. PLGA-DiR NPs were intravenously injected immediately after RIRI or sham surgery in mice. At 12 h after surgery, frozen kidney sections were prepared and stained with phytohemagglutinin-E (PHA-E) for visualizing proximal tubules (a) and phytoagglutin (PNA) for visualizing distal tubules (b). DAPI was used for staining nuclei. Merged views are shown in the right panels. Representative fluorescent images are from three independent experiments showing similar results. Scale bar, 150 μm.

and fibronectin positive areas were significantly lower with IR + PLGA-Oltipraz NPs than other administrations (Fig. 6b), which suggests the anti-fibrosis function of PLGA-Oltipraz NPs in the late stage of RIRI pathogenesis. Meanwhile, we performed histological analysis of the sham-operated groups and found no significant difference in H&E, Masson, and IHC staining between each group (Fig. S1).

The expression of Nrf2 signaling pathway-associated proteins were also examined in kidney tissues. On days 3 and 7 after RIRI, the IR kidneys of five groups were harvested for Western blot analysis. Apart from the high expression of Nrf2 and its downstream proteins in the sham group, renal IR injury could inherently inhibit the Nrf2 signaling pathway at days 3 and 7 after RIRI (Fig. 5c). Oltipraz is a strong Nrf2 activator, however, the activation effect of Oltipraz alone was slight. The expression of Nrf2 and its downstream proteins showed great increase with PLGA-Oltipraz NPs administration, suggesting that Nrf2 signaling pathway could be activated by the PLGA-Oltipraz NPs. Nrf2 is responsible for regulating the cell's antioxidant response via the antioxidant response element and is thought to be involved in the repair and recovery process from AKI [41].

What's more, we evaluated the renal function protection effect of PLGA-Oltipraz NPs in RIRI mice with right kidney dissection. After establishing the RIRI model, PBS, PLGA NPs, Oltipraz, and PLGA-Oltipraz NPs were intravenously injected immediately in the sham control group and AKI group. Both serum creatinine and blood urea nitrogen (BUN) levels were increased 24 h after RIRI (Fig. 5d and e). In hypoxia condition, the BUN content was 222.16 mg/dL and 198.85 mg/dL respectively in PBS and PLGA added cells. Serum BUN level was decreased to 107.28 mg/dL in Oltipraz group compare to that in PBS control group ($p < 0.01$). However, it was significantly lower to 62.71 mg/dL in PLGA-Oltipraz group compare to BUN content in Oltipraz group ($p < 0.05$) (Fig. 5d). The creatinine showed 1.98 mg/dL in PBS and 1.75 mg/dL in PLGA added control cells, while 1.46 mg/dL in

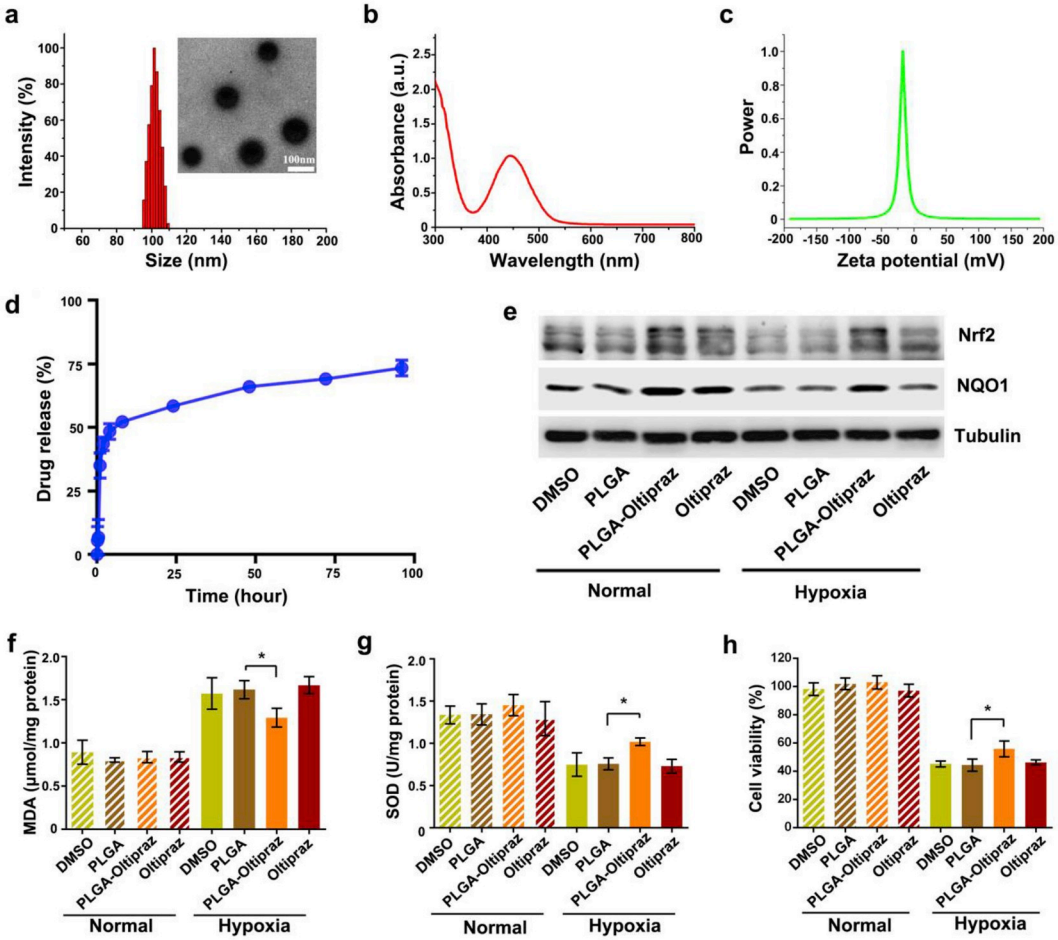

Fig. 4. Characterization of PLGA-Oltipraz NPs and their antioxidant role *in vitro*. (a) Size distribution and colloid stability of PLGA-Oltipraz NPs by dynamic light scattering. Inset: TEM of PLGA-Oltipraz NPs; scale bar, 100 nm. (b) UV–visible absorption spectrum and (c) zeta potential of PLGA-Oltipraz NPs. (d) Oltipraz release profiles of PLGA-Oltipraz NPs. (e) HK2 cells were pretreated separately with PLGA-Oltipraz, PLGA, Oltipraz, and DMSO for 24 h. Normal group cells were cultured in standard medium and room air with 5% CO_2 for 2 h. Hypoxia group cells were cultured in medium without serum and exposed to hypoxia for 1 h, the cultures were replaced with standard medium and allowed to recover in room air with 5% CO_2 for 1 h. Western blot analysis of the effect of DMSO, PLGA, PLGA-Oltipraz or Oltipraz NPs on Nrf2 and downstream NQO1 (the protein levels were normalized to Tubulin level). (f) Malondialdehyde (MDA) levels by thiobarbituric acid assay. (g) Superoxide dismutase (SOD) levels by WST-8 assay. (h) Cell viability by CCK-8 assay. *P < 0.05, *t*-test.

Oltipraz and 1.03 mg/dL in PLGA-Oltipraz treated cells during hypoxia. The creatinine level in PLGA-Oltipraz treated cells was decreased compared to that in PLGA treated cells ($p < 0.05$). Moreover, it was significantly lower in PLGA-Oltipraz group compared to creatinine in Oltipraz group ($p < 0.05$) (Fig. 5e). The results suggest that the PLGA-Oltipraz NPs are effective on protecting renal function at the initial phase of AKI. Overall, we demonstrated that at the initial phase of renal IR injury, PLGA-Oltipraz NPs (100 nm) passed through the impaired GFB, accumulated in renal tubules and were taken up by renal tubular epithelial cells. Then, Oltipraz were gradually released from the NPs, activating the expression of anti-oxidative stress-related Nrf2 and its downstream targets NQO1, GCLC, and Gpx2, which reduced the tubular damage and alleviated renal fibrosis.

We further evaluated the potential toxicity of PLGA NPs on major organs (heart, liver, spleen, and lung) after RIRI (Fig. S2). We harvested the major organs from sham-operated and RIRI mice treated with PBS, PLGA, single Oltipraz and PLGA-Oltipraz NPs. H&E-stained sections of the four tissues (heart, liver, spleen and lung) showed no apparent lesions (no necrosis, edema, inflammatory infiltration and hyperplasia) in either group. Thus, PLGA-Oltipraz NPs administration did not induce significant damage to major organs.

Currently no effective treatment is available for AKI in clinic even after investigating for decades. Instead of developing more effective agents, many efforts were made by improving the treatment strategies with nanotechnology. The GFB becomes the greatest barrier to deliver agents to renal tubules. Though newly designed nanoparticles could pass through GFB and target to the renal tubules, they were still far away from clinical application. In the present study, we found a "therapeutic window" during AKI, which enable us to effectively deliver agents to renal tubular epithelial cells with FDA approved starting materials.

4. Conclusion

In summary, we fabricated biocompatible PGLA-based Oltipraz NPs with the ability of forming high accumulation in the IR kidney and targeting renal tubules for treating IR-induced AKI. PLGA-Oltipraz NPs represent a passive target route for injured kidneys after RIRI with strict particle-size selection. The high NPs accumulation in IR kidneys enables concentrated release of encapsulated drugs *in situ* to alleviate the inflammatory damage caused by IR and reduce renal fibrosis. The designed NPs could be a promising treatment strategy for IR-induced AKI and significant potential in clinical translation can be predicted.

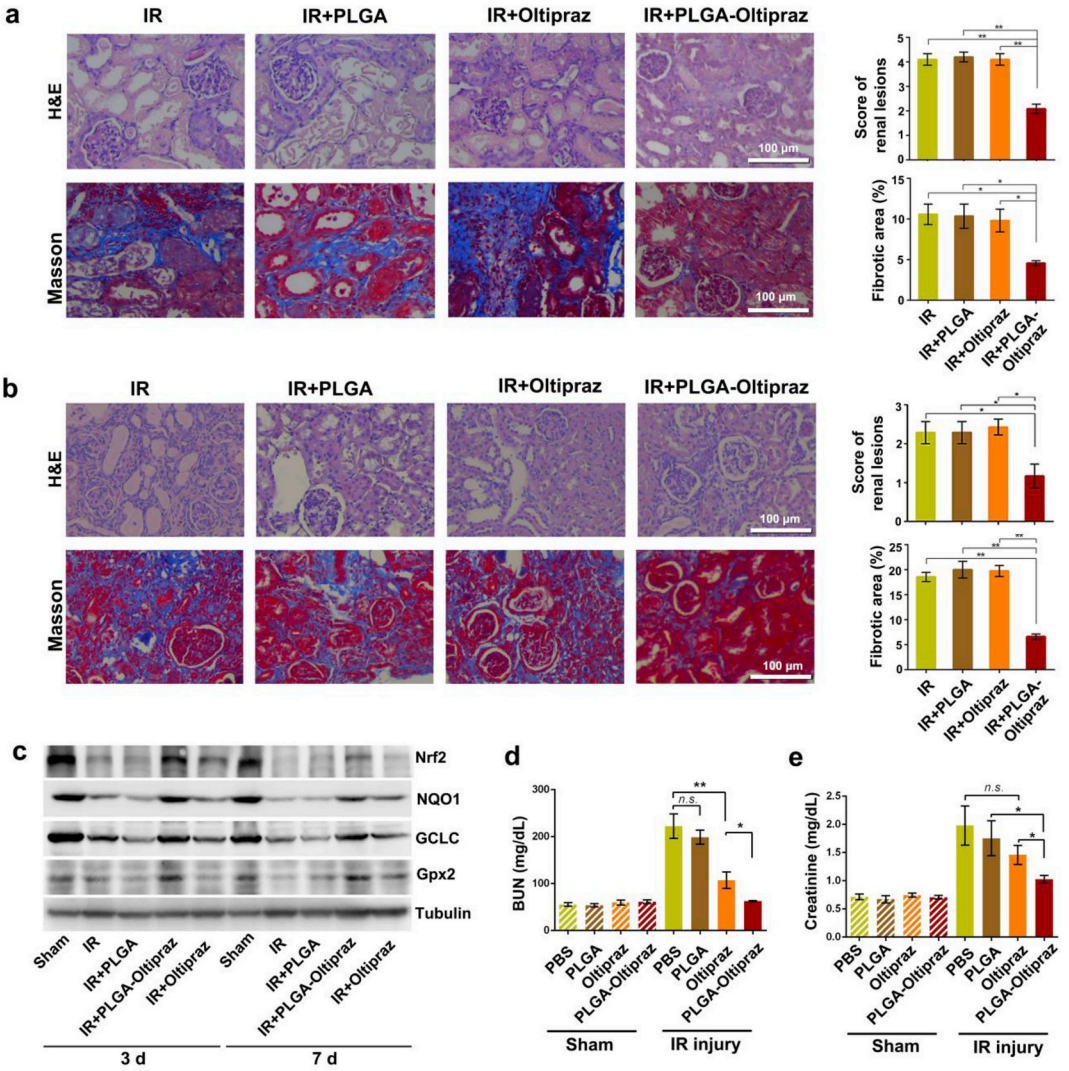

Fig. 5. Histological analysis of the IR kidneys. (a) IR kidneys on day 3 after RIRI were prepared and analyzed. Representative images and histological score of H&E and Masson staining in each group. (b) After 6 weeks, injury kidneys were collected and prepared for histological analysis. Representative images and histological score of H&E and Masson staining in each group. (c) Western blot analysis of protein levels of Nrf2 and downstream NQO1, GCLC and Gpx2 in IR mice on days 3 and 7 after RIRI. (d) Blood urea nitrogen (BUN) level and (e) creatinine levels at 24 h in mice with and without AKI. The data are shown as mean ± SD (n = 3). *P < 0.05, **P < 0.01, n.s., not significant, *t*-test.

Associated content

Supporting information

The Supporting Information (SI) includes histological analysis of the kidneys after sham surgery and treatment, and histological analysis of the major organs at 6 weeks after RIRI model and treatment (Figs. S1–S2).

Notes

The authors declare no competing financial interest.

CRediT authorship contribution statement

Hang Yu: Conceptualization, Methodology, Data curation. **Tingsheng Lin:** Conceptualization, Methodology, Software, Writing - original draft. **Wei Chen:** Visualization, Investigation, Writing - review & editing, Supervision. **Wenmin Cao:** Methodology, Data curation, Validation. **Chengwei Zhang:** Methodology, Software, Formal analysis. **Tianwei Wang:** Methodology, Data curation. **Meng Ding:** Writing - review & editing, Supervision. **Sheng Zhao:** Writing - review & editing. **Hui Wei:** Conceptualization, Writing - review & editing. **Hongqian Guo:** Conceptualization, Supervision, Project administration, Funding acquisition. **Xiaozhi Zhao:** Conceptualization, Supervision, Project administration, Funding acquisition.

Acknowledgment

This work was supported by grants from the Project of Invigorating Health Care through Science, Technology and Education Jiangsu Provincial Key Medical Talents QNRC2016015 (to X.Z.), and Key Medical Discipline ZDXKB2016014 (to H.G.), China Postdoctoral Science Foundation 2018M640477 (to X.Z.), Nanjing Health Distinguished Youth Fund JQX15006 (to X.Z.), Nanjing Science and Technology Project 201715025 (to X.Z.).

Appendix A. Supplementary data

Supplementary data to this article can be found online at https://doi.org/10.1016/j.biomaterials.2019.119368.

The above descriptions are accurate and agreed by all authors.

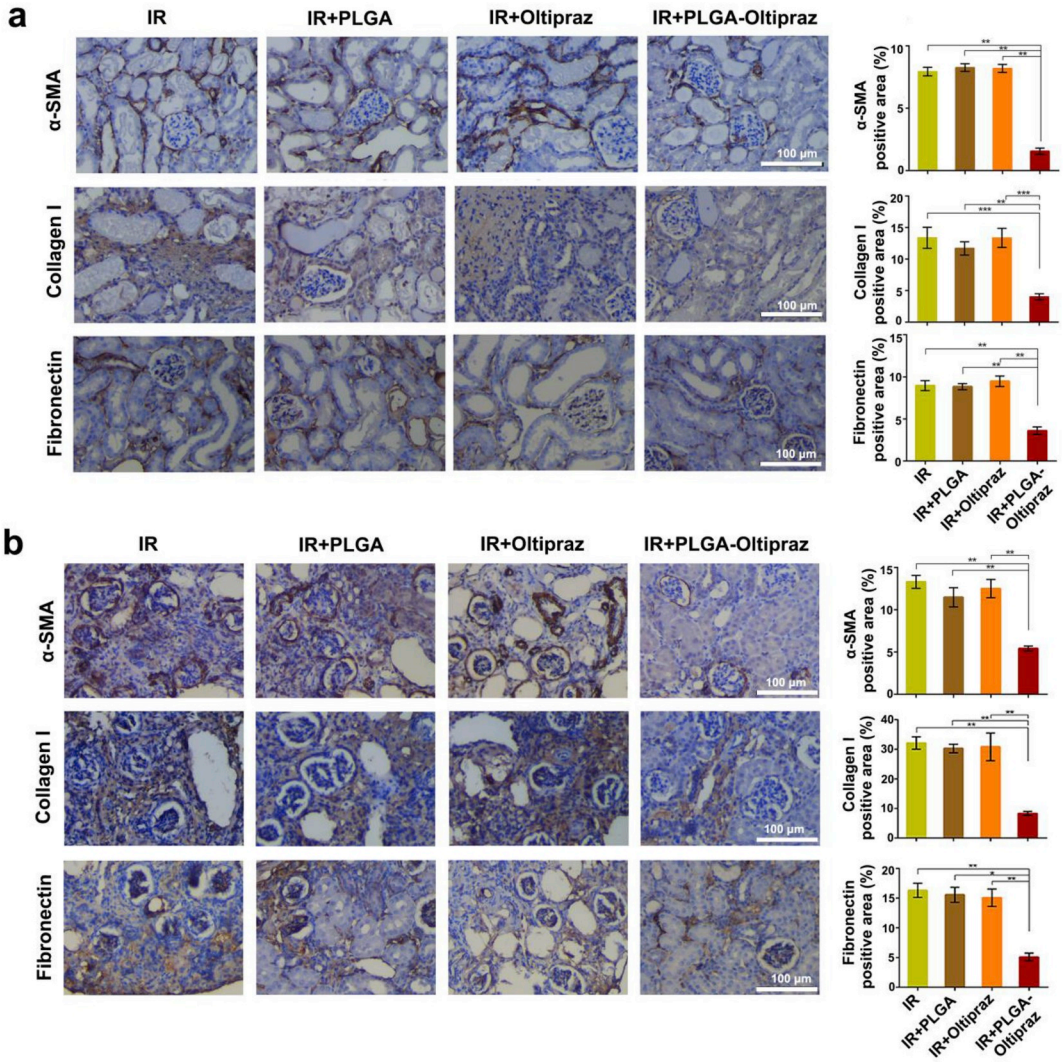

Fig. 6. Histological analysis of the IR kidneys. (a) IR kidneys on day 3 after RIRI were prepared and analyzed. IHC staining and the corresponding percentage of positive areas of α-SMA, collagen I, and fibronectin. Scale bar, 100 μm. (b) After 6 weeks, injury kidneys were collected and prepared for histological analysis. IHC staining and the corresponding percentage of positive areas of α-SMA, collagen I, and fibronectin. Scale bar, 100 μm. The data are shown as mean ± SD (n = 3). *P < 0.05, **P < 0.01, ***P < 0.001, *t*-test.

References

[1] E.A.J. Hoste, J.A. Kellum, N.M. Selby, A. Zarbock, P.M. Palevsky, S.M. Bagshaw, et al., Global epidemiology and outcomes of acute kidney injury, Nat. Rev. Nephrol. 14 (2018) 607–625.

[2] A. Zuk, J.V. Bonventre, Acute kidney injury, Annu. Rev. Med. 67 (2016) 293–307.

[3] N.H. Lameire, A. Bagga, D. Cruz, J. De Maeseneer, Z. Endre, J.A. Kellum, et al., Acute kidney injury: an increasing global concern, Lancet 382 (2013) 170–179.

[4] E.A. Hoste, S.M. Bagshaw, R. Bellomo, C.M. Cely, R. Colman, D.N. Cruz, et al., Epidemiology of acute kidney injury in critically ill patients: the multinational AKI-EPI study, Intensive Care Med. 41 (2015) 1411–1423.

[5] D.A. Ferenbach, J.V. Bonventre, Mechanisms of maladaptive repair after AKI leading to accelerated kidney ageing and CKD, Nat. Rev. Nephrol. 11 (2015) 264–276.

[6] M. Matejovic, C. Ince, L.S. Chawla, R. Blantz, B.A. Molitoris, M.H. Rosner, et al., Renal hemodynamics in AKI: in search of new treatment targets, J. Am. Soc. Nephrol. 27 (2016) 49–58.

[7] B.C. Liu, T.T. Tang, L.L. Lv, H.Y. Lan, Renal tubule injury: a driving force toward chronic kidney disease, Kidney Int. 93 (2018) 568–579.

[8] K.C. Leung, M. Tonelli, M.T. James, Chronic kidney disease following acute kidney injury-risk and outcomes, Nat. Rev. Nephrol. 9 (2013) 77–85.

[9] M.U. Sharif, M.E. Elsayed, A.G. Stack, The global nephrology workforce: emerging threats and potential solutions!, Clin. Kidney J. 9 (2016) 11–22.

[10] N. Kamaly, J.C. He, D.A. Ausiello, O.C. Farokhzad, Nanomedicines for renal disease: current status and future applications, Nat. Rev. Nephrol. 12 (2016) 738–753.

[11] R.M. Williams, E.A. Jaimes, D.A. Heller, Nanomedicines for kidney diseases, Kidney Int. 90 (2016) 740–745.

[12] G.T. Tietjen, S.A. Hosgood, J. DiRito, J. Cui, D. Deep, E. Song, et al., Nanoparticle targeting to the endothelium during normothermic machine perfusion of human kidneys, Sci. Transl. Med. 9 (2017).

[13] J. Wang, J.J. Masehi-Lano, E.J. Chung, Peptide and antibody ligands for renal targeting: nanomedicine strategies for kidney disease, Biomater. Sci. 5 (2017) 1450–1459.

[14] R.M. Williams, J. Shah, B.D. Ng, D.R. Minton, L.J. Gudas, C.Y. Park, et al., Mesoscale nanoparticles selectively target the renal proximal tubule epithelium, Nano Lett. 15 (2015) 2358–2364.

[15] S. Gao, S. Hein, F. Dagnaes-Hansen, K. Weyer, C. Yang, R. Nielsen, et al., Megalin-mediated specific uptake of chitosan/siRNA nanoparticles in mouse kidney proximal tubule epithelial cells enables AQP1 gene silencing, Theranostics 4 (2014) 1039–1051.

[16] M.G. Lawrence, M.K. Altenburg, R. Sanford, J.D. Willett, B. Bleasdale, B. Ballou, et al., Permeation of macromolecules into the renal glomerular basement membrane and capture by the tubules, Proc. Natl. Acad. Sci. U. S. A. 114 (2017) 2958–2963.

[17] C. von Roemeling, W. Jiang, C.K. Chan, I.L. Weissman, B.Y.S. Kim, Breaking down the barriers to precision cancer nanomedicine, Trends Biotechnol. 35 (2017) 159–171.

[18] S. Satchell, The role of the glomerular endothelium in albumin handling, Nat. Rev. Nephrol. 9 (2013) 717–725.

[19] S. Alidori, N. Akhavein, D.L. Thorek, K. Behling, Y. Romin, D. Queen, et al., Targeted fibrillar nanocarbon RNAi treatment of acute kidney injury, Sci. Transl. Med. 8 (2016) 331–339.

[20] H. Qiao, M. Sun, Z. Su, Y. Xie, M. Chen, L. Zong, et al., Kidney-specific drug delivery system for renal fibrosis based on coordination-driven assembly of catechol-derived chitosan, Biomaterials 35 (2014) 7157–7171.

[21] D. Jiang, Z. Ge, H.J. Im, C.G. England, D. Ni, J. Hou, et al., DNA origami nanostructures can exhibit preferential renal uptake and alleviate acute kidney injury,

Nat. Biomed. Eng. 2 (2018) 865–877.
[22] M. Malek, M. Nematbakhsh, Renal ischemia/reperfusion injury; from pathophysiology to treatment, J. Ren. Inj. Prev. 4 (2015) 20–27.
[23] M. Andersson, U. Nilsson, C. Hjalmarsson, B. Haraldsson, J.S. Nystrom, Mild renal ischemia-reperfusion reduces charge and size selectivity of the glomerular barrier, Am. J. Physiol. Renal. Physiol. 292 (2007) 1802–1809.
[24] S.I. Tyritzis, M. Zachariades, K. Evangelou, V.G. Gorgoulis, A. Kyroudi-Voulgari, K. Pavlakis, et al., Effects of prolonged warm and cold ischemia in a solitary kidney animal model after partial nephrectomy: an ultrastructural investigation, Ultrastruct. Pathol. 35 (2011) 60–65.
[25] C. Rippe, A. Rippe, A. Larsson, D. Asgeirsson, B. Rippe, Nature of glomerular capillary permeability changes following acute renal ischemia-reperfusion injury in rats, Am. J. Physiol. Renal. Physiol. 291 (2006) 1362–1368.
[26] L.M. Shelton, B.K. Park, I.M. Copple, Role of Nrf2 in protection against acute kidney injury, Kidney Int. 84 (2013) 1090–1095.
[27] M. Nezu, T. Souma, L. Yu, T. Suzuki, D. Saigusa, S. Ito, et al., Transcription factor Nrf2 hyperactivation in early-phase renal ischemia-reperfusion injury prevents tubular damage progression, Kidney Int. 91 (2017) 387–401.
[28] S. Ruiz, P.E. Pergola, R.A. Zager, N.D. Vaziri, Targeting the transcription factor Nrf2 to ameliorate oxidative stress and inflammation in chronic kidney disease, Kidney Int. 83 (2013) 1029–1041.
[29] J.M. Chan, L. Zhang, K.P. Yuet, G. Liao, J.W. Rhee, R. Langer, et al., PLGA-lecithin-PEG core-shell nanoparticles for controlled drug delivery, Biomaterials 30 (2009) 1627–1634.
[30] L. Zhang, J.M. Chan, F.X. Gu, J.W. Rhee, A.Z. Wang, A.F. Radovic-Moreno, et al., Self-assembled lipid–polymer hybrid nanoparticles: a robust drug delivery platform, ACS Nano 2 (2008) 1696–1702.
[31] B. Tampe, U. Steinle, D. Tampe, J.L. Carstens, P. Korsten, E.M. Zeisberg, et al., Low-dose hydralazine prevents fibrosis in a murine model of acute kidney injury-to-chronic kidney disease progression, Kidney Int. 91 (2017) 157–176.
[32] L. Ge, W. Chen, W. Cao, G. Liu, Q. Zhang, J. Zhuang, et al., GCN2 is a potential prognostic biomarker for human papillary renal cell carcinoma, Cancer Biomark. 22 (2018) 395–403.
[33] C. Yuste, E. Gutierrez, A.M. Sevillano, A. Rubio-Navarro, J.M. Amaro-Villalobos, A. Ortiz, et al., Pathogenesis of glomerular haematuria, World J. Nephrol. 4 (2015) 185–195.
[34] H. Castrop, I.M. Schiessl, Novel routes of albumin passage across the glomerular filtration barrier, Acta Physiol. 219 (2017) 544–553.
[35] W. Wang, G. Ramesh, Segment-specific expression of netrin-1 receptors in normal and ischemic mouse kidney, Am. J. Nephrol. 30 (2009) 186–193.
[36] Q. Ma, Role of nrf2 in oxidative stress and toxicity, Annu. Rev. Pharmacol. Toxicol. 53 (2013) 401–426.
[37] M.S. Joo, C.G. Lee, J.H. Koo, S.G. Kim, miR-125b transcriptionally increased by Nrf2 inhibits AhR repressor, which protects kidney from cisplatin-induced injury, Cell Death Dis. 4 (2013) e899.
[38] A. Atilano-Roque, X. Wen, L.M. Aleksunes, M.S. Joy, Nrf2 activators as potential modulators of injury in human kidney cells, Toxicol Rep 3 (2016) 153–159.
[39] W. Kong, J. Fu, N. Liu, C. Jiao, G. Guo, J. Luan, et al., Nrf2 deficiency promotes the progression from acute tubular damage to chronic renal fibrosis following unilateral ureteral obstruction, Nephrol. Dial. Transplant. 33 (2018) 771–783.
[40] M.J. Moeller, V. Tenten, Renal albumin filtration: alternative models to the standard physical barriers, Nat. Rev. Nephrol. 9 (2013) 266–277.
[41] M. Liu, N.M. Reddy, E.M. Higbee, H.R. Potteti, S. Noel, L. Racusen, et al., The Nrf2 triterpenoid activator, CDDO-imidazolide, protects kidneys from ischemia-reperfusion injury in mice, Kidney Int. 85 (2014) 134–141.